Adiabatic Nanofocusing on Ultrasmooth Single-Crystalline Gold Tapers Creates a 10-nm-Sized Light Source with Few-Cycle Time Resolution

Slawa Schmidt,[†] Björn Piglosiewicz,[†] Diyar Sadiq,[†] Javid Shirdel,[†] Jae Sung Lee,[‡] Parinda Vasa,[†] Namkyoo Park,[‡] Dai-Sik Kim,[§] and Christoph Lienau[†,*]

[†]Institut für Physik, Carl von Ossietzky Universität, 26111 Oldenburg, Germany, [‡]Photonic Systems Laboratory, School of EECS, Seoul National University, Seoul 151-744, Korea, and [§]Center for Subwavelength Optics and Department of Physics and Astronomy, Seoul National University, Seoul 151-747, Korea

ABSTRACT

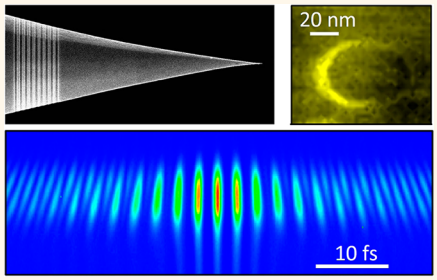

We demonstrate adiabatic nanofocusing of few-cycle light pulses using ultrasharp and ultrasmooth single-crystalline gold tapers. We show that the grating-induced launching of spectrally broad-band surface plasmon polariton wavepackets onto the shaft of such a taper generates isolated, point-like light spots with 10 fs duration and 10 nm diameter spatial extent at its very apex. This nanofocusing is so efficient that nanolocalized electric fields inducing strong optical nonlinearities at the tip end are reached with conventional high repetition rate laser oscillators. We use here the resulting second harmonic to fully characterize the time structure of the localized electric field in frequency-resolved interferometric autocorrelation measurements. Our results strongly suggest that these nanometer-sized ultrafast light spots will enable new experiments probing the dynamics of optical excitations of individual metallic, semiconducting, and magnetic nanostructures.

KEYWORDS: ultrafast nano-optics · adiabatic nanofocusing · surface plasmon polaritons · metallic nanostructures · second harmonic generation

Metallic nanostructures have remarkable optical properties. Depending on their geometry, their optical spectra are governed either by propagating surface plasmon polariton (SPP) resonances,[1] such as in planar layers, by localized surface plasmon (LSP) resonances,[2] such as in invidual nanoparticles, or by combinations thereof. Conceptually, this offers, in favorable geometries, the possibility to coherently transport energy in the form of SPP waves over mesoscopic distances and to guide and localize this energy into nanometric spots by coupling SPPs to LSPs.[3−8] Such a nanofocusing of SPP waves is of immediate interest for a variety of applications, ranging from ultra-high-resolution optical microscopy,[9,10] tip-enhanced Raman spectroscopy,[11] or extreme ultraviolet (EUV) generation[12] to quantum information processing.[13] Nanofocusing is expected to be particularly efficient in the adiabatic limit[5,6] in which changes in SPP wavevector are small on a length scale of the SPP wavelength and radiative as well as reflective losses are minimized. Experimentally, adiabatic nanofocusing has recently been studied in a variety of different geometries such as two-dimensional tapered waveguides,[14,15] metallic grooves,[16] and three-dimensional conical tapers.[9−11,17] In particular, sharp conical gold tapers with nanoslit gratings milled onto the taper shaft[9−11,17] are of interest. In such structures, far-field illumination of the grating can be used for launching SPP waves that then propagate toward the very apex of the tip. Here, this creates a bright and spatially isolated nanometer-sized light source, ideal for applications, such as in scattering-type near-field scanning optical microscopy (s-NSOM). So far, most of the research efforts in this field have focused on studying the spatial aspects of such adiabatically nanofocused light spots, while first dynamical studies of adiabatic nanofocusing appeared only very recently.[18] Such time-resolved studies are needed for exploiting the full potential of such tapers for creating isolated few-nanometer-sized light spots with few-cycle time resolution, an important tool for time-resolved nanoparticle spectroscopy.

* Address correspondence to christoph.lienau@uni-oldenburg.de.

Received for review March 14, 2012 and accepted June 8, 2012.

Published online June 08, 2012
10.1021/nn301121h

On the theoretical side, adiabatic concentration of ultrashort SPP pulses in metallic wedges[19] and more complicated nanostructures[20] has recently been studied in some detail on the basis of general time reversal ideas.[21] In wedges,[22] a nanofocused ultrashort pulse with the desired temporal profile is back-propagated from the taper apex into the launching region. This provides the amplitude and phase profile for each constituent frequency at well-defined spatial positions on the nanostructure surface that is needed to form the nanolocalized light spot. Nontrivial spatio-spectral phase profiles are obtained, suggesting the use of advanced pulse shaping technology for creating the desired input light fields. Indeed, in their initial experiments, Berweger *et al.*[18] employed a spatial light modulator with independent spectral amplitude and phase control for obtaining pulses confined to 20 nm with 16 fs time duration at the tip apex. Evidently, the need for complex pulse shaping makes applications of such nanofocused light spots more difficult, and it might be helpful to avoid this complexity. Previous nanofocusing experiments have been performed using inherently rough, chemically etched multicrystalline gold tapers.[23] Even though fairly little is actually known experimentally[24] and theoretically[25–27] about the losses and dispersion of few-cycle SPP pulses while propagating along such surfaces, one may expect that surface roughness and grain boundaries in multicrystalline tapers[28,29] will result in substantial out-of plane radiative losses[30] and in-plane k-vector mixing. This would result in additional pulse dispersion, increasing the need for external dispersion compensation. Recent studies of silver nanowires provide upper bounds for the SPP group delay dispersion of 50 fs^2 rad^{-1} μm^{-1}.[31]

In the present article, we introduce a novel concept for fabricating ultrasmooth plasmonic conical gold tapers formed by electrochemical etching of single-crystalline gold wires. This allows us to demonstrate 3D adiabatic nanofocusing of ultrafast SPP pulses at the apex of such tapers with 10 nm spatial resolution and 10 fs temporal resolution without the need for spatio-temporal pulse shaping. Adiabatically focused s-NSOM[10] imaging of individual metallic nanoparticles reveals sharp field localization with intensities that are sufficient to induce strong optical nonlinearities at the taper apex. By recording interferometric frequency-resolved autocorrelation (IFRAC) traces of the second harmonic radiation from the tip apex, pulse durations of 10 fs are demonstrated, limited by the acceptance bandwidth of the grating coupler. Our results are strongly supported by three-dimensional time-resolved simulations of SPP pulse propagation on conical gold tapers. This opens the door for exploring extreme nonlinear optical phenomena at the taper apex and for probing the dynamics of optical excitations of single nanostructures with ultrahigh time resolution.

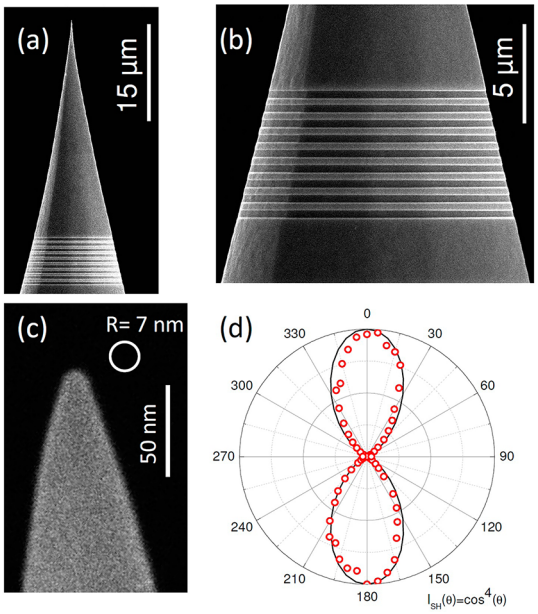

Figure 1. (a) Scanning electron micrograph of a conical monocrystalline gold taper with an 800 nm grating period prepared by focused ion beam milling. (b) Zoomed-in image for the nanoslit grating milled onto the ultrasmooth shaft of the gold taper. (c) Zoomed-in image from the apex of the taper shown in (a) with a radius of only of 7 nm. (d) Second harmonic signal $I_{SH}(\theta)$ (red circles) generated by adiabatic nanofocusing of a SPP wavepacket at the tip apex as a function of the polarization direction θ of the fundamental laser beam with respect to taper axis. A fit of a $\cos^4(\theta)$ dependence to the experimental data is shown as a solid line.

RESULTS AND DISCUSSION

Adiatiabatic Nanofocusing on Single-Crystalline Gold Tapers. The main aim of this work is to study adiabatic nanofocusing of ultrafast SPP pulses on smooth, single-crystalline conical gold tapers. Previously used polycrystalline gold tips contain randomly varying grain sizes and surface roughness on a scale much below the wavelength.[23,24] We expect that, for such tips, the propagation of ultrashort SPP wavepackets with pulse durations in the 10 fs range and typical spectral bandwidths exceeding 200 nm is affected by Rayleigh scattering of SPP modes at grain boundaries and/or surface roughness. We thus used an annealing method prior to etching for obtaining single-crystalline gold wires with smooth surfaces.[23] Polycrystalline 125 μm gold wires are annealed at 800 °C for 8 h and cooled slowly to room temperature, effectively replacing the initially abundant small grains with larger grains comparable to the desired size of the tip shaft. After electrochemical etching of such an annealed wire, we find that in most cases the taper end consists of only one large single crystal, with a smooth and defect-free surface. A scanning electron microscope image of such a plasmonic taper with a grating on its shaft is shown in Figure 1a. Here, the etching parameters were chosen to give an almost perfectly conically shaped taper with an opening angle of 30°. Using such annealed wires,

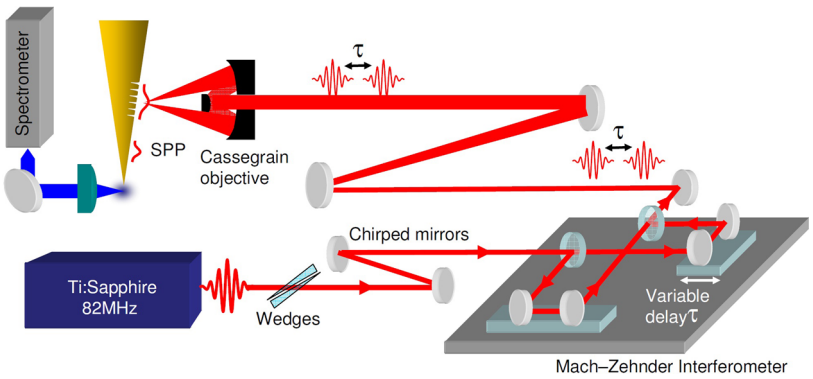

Figure 2. Schematic of the interferometric frequency-resolved autocorrelation (IFRAC) microscope for time-resolved characterization of adiabatically nanofocused plasmonic light spots at the apex of a gold tip. A pair of 6 fs optical pulses centered at 870 nm with variable time delay τ is derived from a mode-locked Ti:sapphire oscillator operating at 82 MHz repetition rate and generated in a dispersion-balanced Mach−Zehnder interferometer. The pulses are focused by an all-reflective Cassegrain objective onto a nanoslit grating milled onto the shaft of the gold taper. Light scattered from the tip apex into the far-field is collected by a second high NA objective in reflection geometry, spectrally dispersed in a monochromator and detected with a cooled CCD detector as a function of the time delay τ between both pulses.

highly reproducible taper geometries are obtained provided that clean chemicals and a vibration-free etching environment are used. For our optical experiments, slit gratings with an 800 nm period, a slit width of 400 nm, and a depth of 100 nm are focused ion beam milled onto the smooth shaft of gold tip at a distance of 30 μm from the tip apex. We have chosen a distance of 30 μm between nanoslit and tip apex in order to separate light scattering from the grating and from the tip apex using far-field optics.[17] This distance is a trade-off between the propagation losses and the reduction in the background signal due to scattering from the grating. For planar single-crystalline Au surfaces, the SPP propagation distance is more than 60 μm at 800 nm[28]—compared to less than 10 μm for multicrystalline samples—so that we expect reasonably small propagation losses. In the chosen geometry, the grating scattering background is negligible. Figure 1b shows a zoomed-in scanning electron microscope image of the nanoslit grating with 800 nm period milled onto the taper shaft. We have examined different slit widths and depths for the gratings for getting higher coupling efficiency and found that a combination of 400 nm width and 100 nm depth gave an optimum coupling efficiency while maintaining a reasonably short pulse duration. A high-resolution image of the taper apex is seen in Figure 1c. It shows a tip with a particularly smooth surface and a radius of curvature at the tip apex of only 7 nm for a taper opening angle of about 30°. We have found that opening angles between 20 and 30° are most efficient in adiabatic nanofocusing. To our knowledge, the surface quality of these etched single-crystalline tapers is superior to that of tapers fabricated by other techniques.

To study the optical properties of these tapers, we use the setup schematically shown in Figure 2. A Ti:sapphire oscillator operating at a repetition rate R of 82 MHz is used to generate 6 fs pulses centered at 870 nm with a pulse energy of 3.7 nJ. Their dispersion is compensated by a pair of chirped mirrors and a wedge pair for fine adjustment. A pair of identical pulses with variable time delay τ is created in a dispersion-balanced Mach−Zehnder interferometer. These pulses are focused at normal incidence to a spot size of 1−2 μm onto the nanoslit grating. For dispersion-free focusing of such broad-band pulses with bandwidth exceeding 200 nm, an all-reflective Cassegrain objective is used.[32] In order to maximize the SPP coupling efficiency, the laser pulses are linearly polarized in the direction perpendicular to the nanoslit gratings. As is well-known, the grating transfers momentum $k_g = 2\pi/a$, where a is the grating period, to the incident light, thus allowing to overcome the momentum mismatch between the incident light and the evanescent SPP modes at the taper surface. The launched ultrafast SPP wavepacket then propagates toward the apex of the conical gold taper. Due to the evanescent nature of the SPP mode, this wavepacket cannot emit radiation into the far-field until it reaches the very apex of the taper.[17] The taper apex then acts as a scatterer for SPP waves and hence transforms this taper into an ultrafast nanometer-sized light spot with strong field enhancement at its very apex.

To characterize the optical properties of those tapers, we first study the overall conversion efficiency between the incident far-field laser light and light scattering from the tip apex. For this, we use a second objective (NA = 0.7) oriented at 90° with respect to the tip axis and collect solely the light scattered from the tip apex. When coupling such short and broad-band pulses onto the grating, we find, for average powers of up to ~5 mW, a linear increase in tip-scattered light with incident power. Higher incident powers are close to the destruction threshold of either the grating or the tip. For an input power of 1.5 mW, typical for that used

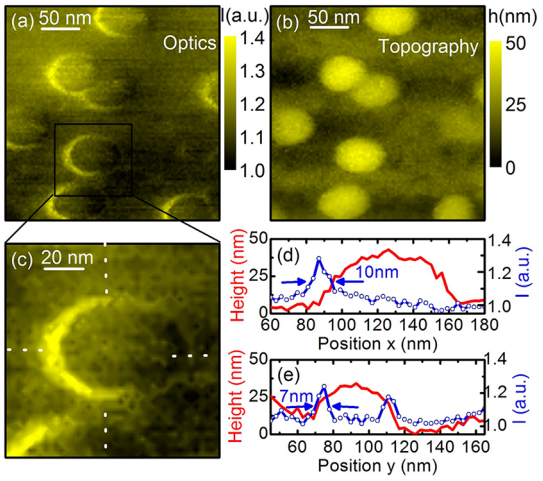

Figure 3. (a) Two-dimensional adiabatically focused s-NSOM image with 10 nm optical resolution of elliptical gold nanoparticles with 60 × 40 × 40 nm³ dimensions on a glass substrate. Strong scattering intensity is only seen at the rim of the nanoparticle, whereas its center remains dark. (b) Corresponding shear force topographical image of the nanoparticles. (c) Close-up image for the nanoparticle indicated by the square in (a). (d,e) Cross sections of the topographical (solid red line) and the optical intensity (opened circles connected by a blue line) along the *x*- and *y*-directions. The cross sections are taken along the dashed lines (c).

in the nonlinear experiments described below, we detect ~1 μW of tip-scattered light in the far-field. Considering the finite collection and detection efficiency of our setup, this suggests that an average power $\bar{P} \sim 10\,\mu$W is emitted from the nanometer-sized apex. This corresponds to a coupling efficiency of 0.7%. We typically obtain coupling efficiencies of 0.3 to 1% for such line gratings. For a pulse duration τ_p = 10 fs, $\bar{P} \sim 10\,\mu$W corresponds to an average peak power of $\bar{P}_p = \bar{P}/(\tau_p R)$ = 12 W or ~10^6 photons per pulse. In comparison to typical photon numbers emitted from other background-free nano light sources, such as aperture or tip-on-aperture probes, this is a remarkably larger number.

Treating the tip for simplicity as an oscillating point dipole in vacuum with dipole moment $\vec{p}_T$, emitting an average power of $\bar{P}_p = (|\vec{p}_T|^2/4\pi\varepsilon_0)(\omega^4/3c^3)$ (where c is the speed of light in vacuum, ω is the laser frequency, and ε_0 is the vacuum permittivity), we estimate a dipole moment on the order of 5 × 10^{-23} Cm. In the quasi-static regime, the near-field at position $\vec{r}$ induced by this dipole located at position $\vec{r}_T$ is given by $\vec{E}_T(\vec{r}) = (3(\vec{p}_T\vec{n})\vec{n} - \vec{p}_T)/(4\pi\varepsilon_0|\vec{r} - \vec{r}_T|^3)$, with $\vec{n} = (\vec{r} - \vec{r}_T)/|\vec{r} - \vec{r}_T|$. At a distance of 10 nm, a conservative estimate of the tip radius r_0, this corresponds to an electric field strength of 10^{12} V/m, on the same order as the atomic field strength $E_{at} = q/(4\pi\varepsilon_0 r^2)$ of 6 × 10^{11} V/m. Hence, we expect in such an adiabatic nanofocusing experiment a regime of extreme nonlinear optics, showing a variety of nonlinear phenomena, including higher harmonic generation[12] or particle emission.[33]

Here, we use the second harmonic (SH) emitted from the tip apex to further characterize these tapers. Under similar excitation conditions (6 fs pulses, input powers of 0.2−3 mW), we observe intense, spectrally broad-band SH emission, centered around 430 nm and with a bandwidth of >100 nm. Under such short pulse excitation conditions, the broad-band continuum emission,[34] known to contribute substantially in similar experiments performed with longer laser pulses, is very weak. Since the scattered light collected from the tip end is free from background excitation light, we can directly correlate the power of the collected light at the fundamental and SH. When collecting about 1 μW at the fundamental, a SH power of about 5 pW is detected. Similar values are obtained for several tips and also in earlier reports,[18] corresponding to an effective tip dipole moment at the SH frequency of $\vec{p}_T^{2\omega}$ of 10^{-26} Cm. Assuming that the SH is emitted from a tip area of $\sim\pi r_0^2$, we estimate an effective nonlinear SH surface polarization[35] $P^s_{eff} = \varepsilon_0\chi^{(2)}_{s,\perp\perp\perp}E_T^2 \approx |\vec{p}_T^{2\omega}|/(\pi r_0^2) \approx 3 \times 10^{-11}$ C/m and hence a value of the dominant, surface-normal component $\chi^s_{s,\perp\perp\perp} \approx 10^{-23}$ m²/V of the surface nonlinear susceptibility tensor,[36,37] which is much smaller than earlier estimates.[18,35]

There may be different causes for this discrepancy, including the crudeness of the estimate, possible coating layers on the gold surface, or laser-induced tip modifications. Most obviously, however, this may indicate that we have substantially underestimated either the spatial size or the temporal duration of the nanofocused light pulse. Both effects will be investigated in detail below. First, we analyze the polarization properties of the emitted SH radiation, another good indicator of the optical properties of such nanotips.[9,38] When changing the linear polarization of the incident laser pulses from perpendicular to parallel to the grating, the SH intensity (Figure 1d, red circles) is suppressed by more than 3 orders of magnitude. The dependence on polarization angle θ is even more pronounced than the $\cos(\theta)^n$, n = 4, dependence (solid line), which is expected when considering only that the linear polarizability tensor of such tips is dominated by its diagonal component along the taper axis[35] and hence $\vec{p}_T$ is also oriented along that direction. The pronounced $n > 4$ dependence found experimentally results from the additional polarization dependence of the grating coupling.

Spatial Characteristics of the Nanofocused Light Spot: Microscopy of Single Metal Nanoparticles. To study the confinement of the adiabatically nanofocused light at the taper apex, we use this spot as a nanolight source in a scattering-type near-field microscope, mapping the optical properties of individual gold nanoparticles.[10] In these experiments, the grating is illuminated with slightly longer 20 fs pulses centered at 800 nm. The light scattered from the apex region is collected while raster-scanning the surface of a quartz substrate

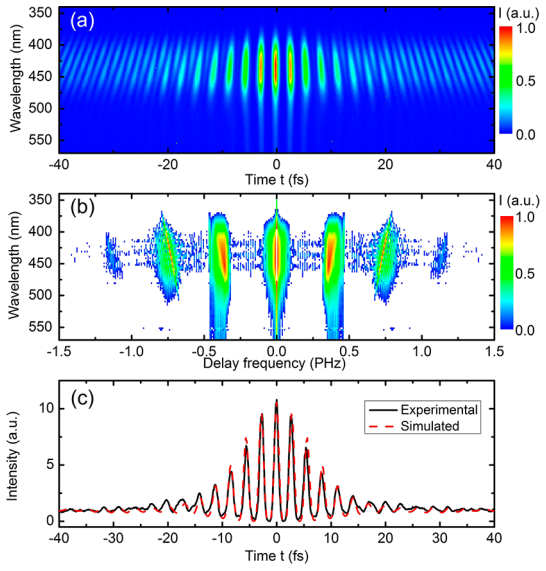

Figure 4. (a) Experimental IFRAC trace from an adiabatically nanofocused plasmonic light spot at the apex of a gold tip. Detection wavelength dependent interference fringes observed in the wavelength range between 390 and 490 nm are the signature of a coherent second harmonic emission process. (b) Spectral Fourier transformations of the IFRAC trace in part (a). (c) Interferometric autocorrelation (IAC) trace (solid, black) obtained by spectrally integrating the data in (a) from 360 to 500 nm and (dashed, red) simulation of the measured IAC trace, indicating a pulse duration of the focused light spot of 10 fs.

covered with a low concentration of gold nanoparticles relative to the gold taper. Scanning is performed at a constant tip−sample distance of 4 nm. Figure 3 shows the grating-coupled s-NSOM image (a) and the corresponding topographic image (b) obtained from slightly elliptical gold nanoparticles with dimensions of 60 × 40 × 40 nm^3. In the simultaneously recorded shear force topographic image, the elliptical shape of the nanoparticles is clearly resolved. The optical image (a) is markedly different from the topographic one. We see a crescent-moon-like near-field pattern, showing strong localization of the optical signal at the edges of the nanoparticle, particularly enhanced at the side of the nanoparticle oriented toward the collection objective. A close-up s-NSOM image for the nanoparticle indicated by a square in (a) is shown in Figure 3c. Cross sections along the dashed lines of the optical image and the corresponding topographic image are depicted in Figure 3d,e, respectively. Along the *x*-axis, pointing into the direction of the collection objective, we find a strong, localized intensity peak with a full width at half-maximum (fwhm) of 10 nm. The *y*-axis profile shows two peaks of equal intensity, separated by 40 nm and having a fwhm of 7 nm only. The intensity maxima are 30−40% higher than the position-independent background normalized to unity. Similar field enhancements at the rim of a nanoparticle have been seen before, for example, in s-NSOM images of gold nanodisks[39,40] or photoinduced polymerization images of gold spheres.[41] They have been interpreted in terms of the coupling between tip dipole and the induced particle dipole[39] or of the overall near-field enhancement of the particle.[41] Our results suggest that, under the present conditions (tip size much smaller than that of the nanoparticle), the contrast is given by the local coupling between the tip dipole—oriented along the taper (*z*-) axis—and the *z*-component of the vectorial electric near-field[42] enhanced at the rim of the nanoparticle and pointing along the tip axis.[43,44] The obscuration of the signal enhancement on one side of the nanoparticle is likely to reflect a shadowing effect since here the tip is placed between the collecting objective and local emission source. The measurements in Figure 3 clearly reveal the spatial confinement of the adiabatically nanofocused spot at the taper apex to about 10 nm. These measurements, recorded with very sharp single-crystalline gold tapers, show a different image contrast than observed earlier.[10] In those experiments, performed with polycrystalline tips with slightly larger radius of curvature, the optical contrast was similar to the topographic one. We assign this change in image contrast mainly to the different tip diameters used in both experiments. A more detailed analysis of the image contrast will be reported elsewhere.

Temporal Characteristics of the Nanofocused Light Spot: Interferometric Frequency-Resolved Autocorrelation. To directly measure the time structure of the adiabatically nanofocused light spot at the taper apex, we perform interferometric frequency-resolved autocorrelation (IFRAC) measurements of the SH radiation emitted from the taper apex under ultrashort pulse illumination. IFRAC is a well-established technique for characterizing amplitude and phase of optical pulses in the few-cycle regime[45−48] and is becoming increasingly relevant for characterizing local electric fields in nanostructures.[49−51] In our measurements, the nanoslit grating on the taper shaft is illuminated with a pair of collinearly propagating, dispersion-free 6 fs incident pulses with electric field $E_{pi}(t,\tau) = E_i(t) + E_i(t+\tau)$ (where $E_i(t)$ is the electric field of the incident pulses and τ is the time delay). A fraction of it is coupled onto the grating and focused to the taper apex, creating a local field $E_{pT}(t,\tau) = E_T(t) + E_T(t+\tau)$, with $E_T(t)$ being the nanofocused field that we are searching for. This field induces a nonlinear polarization at the taper apex, and the electric field $E_{NL}(t,\tau)$ re-emitted by the material polarization is collected and spectrally dispersed in a monochromator. The scattered intensity $I_{IFRAC}(\lambda_d,\tau) = |\int E_{NL}(t,\tau)\exp(-i2\pi ct/\lambda_d)dt|^2$ from the tip apex is recorded as a function of the time delay τ and the detection wavelength λ_d. In the case of a pure coherent and instantaneous SH process, $E_{NL}(t,\tau) = \chi^{(2)}E_{pT}^2$, with $\chi^{(2)}$ being the dominant component of the second-order nonlinear susceptibility tensor.

Figure 4a shows the resulting IFRAC trace from the grating-coupled plasmonic gold taper, obtained by

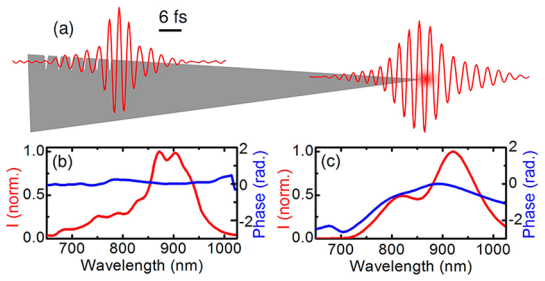

Figure 5. (a) Time profile of the electric field $E_i(t)$ of the incident laser focused onto the grating and the nanofocused field $E_T(t)$ at the taper apex retrieved from IFRAC measurements (Figure 4). The slight temporal stretching of $E_T(t)$ to a pulse duration of ~10 fs is visible. Intensity spectrum $I(\lambda_d)$ and spectral phase $\varphi(\lambda_d)$ of the incident laser (b) and the nanofocused spot (c), respectively. In contrast to the flat spectral phase of the incident pulse, the nanofocused pulse shows a small second-order dispersion of 25 fs^2.

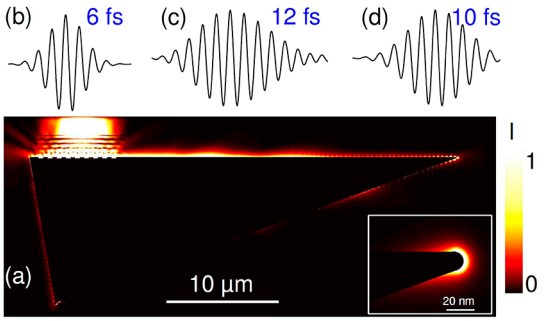

Figure 6. FDTD simulations illustrating adiabatic nanofocusing of ultrafast SPP wavepackets on a grating-coupled plasmonic gold taper. (a) FDTD simulation of the time-averaged electric field intensity on such a plasmonic taper. The inset shows the zoomed-in field image near the tip apex. (b–d) Time structure of the electric field of the (b) incident 6 fs light pulse, (c) 12-fs SPP pulse launched by grating coupling, and (d) resulting 10 fs adiabatically nanofocused SPP pulse at the taper apex.

recording the scattered emission between 340 and 570 nm while varying the interpulse delay time τ between −40 and +40 fs. The IFRAC trace is dominated by the blue SH emission band around 435 nm. It shows a modulation period which varies linearly with λ_d and indicates a coherent nonlinear emission process.[46,50] Even though the SH spectrum extends from 360 to 500 nm, it is slightly narrower than half of the width of the incident laser spectrum covering the wavelength range from 650 to 1050 nm.

To retrieve $E_T(t)$, we analyze the Fourier transform of the IFRAC trace along the delay axis (see Figure 4b). This Fourier transform shows peaks around delay frequencies ν_τ of 0 (the DC component), $\pm c/2\lambda_d$ (the fundamental side bands), and $\pm c/\lambda_d$ (the second-order side bands). In addition, weak peaks at the third side band reveal the presence of higher order harmonic processes.[48,50] In the absence of incoherent emission and assuming quasi-instantaneous material nonlinearites, both the DC component and the fundamental side peak can be used for direct pulse retrieval.[46] We have used the DC component to retrieve $E_T(t)$, and Figure 4c shows that the interferometric autocorrelation (IAC) trace $I_{IAC}(\tau) = \int I_{IFRAC}(\tau,\lambda_d)d\lambda_d$ calculated from $E_T(t)$ agrees well with that obtained from the data in Figure 4a, spectrally integrated between 360 and 500 nm. Similar IFRAC measurements have independently been performed on the incident pulses $E_i(t)$ using a thin BBO crystal for SH generation. The results of the pulse retrieval process are summarized in Figure 5. The incident pulses have a pulse duration of 6 fs (a), defined as the fwhm of the intensity envelope, and their spectral phase is essentially flat (b). Upon grating coupling and propagation toward the tip apex, the pulse duration of $E_T(t)$ is slightly stretched to ~10 fs. At the same time, the intensity spectrum $I_T(\lambda)$ (c) is slightly narrower than the incident spectrum, specifically the short wavelength part is suppressed. The retrieved spectral phase $\varphi_T(\lambda_d)$ (c) shows a slight second-order dispersion of 25 fs^2. This puts an upper bound on the dispersion of the SPP wavepacket experienced while propagating over 30 μm along the taper.

To interpret these experimental results, we compare them to fully three-dimensional finite-difference time domain (FDTD) simulations. In the simulations, the tip is considered as a conical gold taper with an opening angle of 20° and a tip apex radius of 7 nm. The grating parameters are the same as in the experiment, and a Drude model is used for calculating the dielectric function of gold. Due to the large required computational space, varying grid sizes are used with a size of 0.2 nm around the tip apex.

Figure 6a shows an image of the time-averaged electric field intensity simulated when focusing a 6 fs pulse to a 4 μm spot size on the grating, separated by 30 μm from the taper apex. A movie of the corresponding time evolution of the local field intensity is shown in the Supporting Information. The simulations give clear evidence for adiabatic nanofocusing (see inset in Figure 6a) and predict a field intensity at a distance of 5 nm from the taper apex, which is ~200 times larger than the incident intensity. This compares well with the intensity enhancement factor of 100 deduced from the experimental parameters for a tip size of 10 nm. The simulations now allow us to extract the time structure of $E(t)$ at different positions on the taper. Figure 6b,c shows that the grating coupling transforms the incident 6 fs pulse into a 12 fs pulse when measured at a distance of 28 μm from the apex. Upon nanofocusing, the time structure of $E(t)$ changes only slightly. A movie provided as Supporting Information shows a break-up of the pulse into components propagating on the front and back side of the taper. The pulse duration at the taper apex is even slightly shortened to 10 fs, as illustrated in Figure 6d. Our calculations suggest that this reduction in pulse duration may result from transforming different parts of the incident laser spectrum into SPP at different positions on the grating. In general,

the predicted pulse duration matches well with experiment. We take this as a strong indication that under our experimental conditions the acceptance bandwidth of the grating coupler, rather than pulse dispersion upon SPP propagation, limits the achievable time resolution in adiabatic nanofocusing. Even for long, 30 μm propagation distances and few-cycle light pulses, SPP dispersion is small for the ultrasmooth single-crystalline tapers introduced in this work. The measured dispersion of 25 fs^2 would result in a stretching of a chirp-free 6 fs pulse to less than 12 fs. This effectively alleviates the need for advanced pulse shaping techniques for creating adiabatically nanofocused light pulses with few-cycle time resolution.

Summary and Conclusion. In summary, we have introduced novel ultrasmooth and ultrasharp single-crystalline gold tapers for exploring, both experimentally and theoretically, grating coupling, propagation, and adiabatic nanofocusing of ultrashort few-cycle SPP pulses. We demonstrate nanofocused pulses at the taper apex with a duration of only 10 fs, spatially localized to about 10 nm. This nanofocusing is so efficient that intense optical fields, inducing strong optical nonlinearities at the tip apex, are generated by high repetition rate laser oscillators. We use the induced second harmonic emission from the taper apex for retrieving amplitude and spectral phase of the focused light spot. This allows us to directly measure the dispersion of ultrashort SPP pulses propagating in nanoconfined geometries. We provide an upper bound of 25 fs^2 for the chirp acquired within a 30 μm propagation distance. Our results open up different interesting perspectives for future work. First of all, they indicate a new method for probing ultrafast SPP propagation[52] and dispersion in metallic nanostructures, a topic which so far has not yet been studied in much detail. Here, it will be particularly interesting to compare our findings to studies of SPP on polycrystalline metal interfaces. Moreover, it is immediately apparent that such intense and isolated few-cycle nanofocused light pulses are of substantial interest for a variety of applications in nanoimaging and spectroscopy, in particular, for probing optical nonlinearities and dynamics of optical excitations in nanostructures.

METHODS

Single-Crystalline Gold Tapers. Polycrystalline gold wires (99.99%) with a diameter of 125 μm are purchased from Advent Research Materials Ltd., Oxford, UK, and cleaned in ethanol. The wires are annealed at 800 °C for 8 h and then slowly cooled to room temperature.[23] These annealed wires are then electrochemically etched in HCl (aq. 37%). For etching, rectangular voltage pulses with a frequency of 3 kHz and a duty cycle of 10% are applied between the wire and a platinum ring serving as the counter electrode similar to what has been described earlier.[53] The tip shape is inspected by scanning electron microscopy. Gratings are milled onto the shaft of these tapers in a dual-beam focused ion beam microscope (FEI Helios 600i).

Interferometric Frequency-Resolved Autocorrelation Microscopy. A schematic of the experimental setup used in this work is shown in Figure 2. It is based on a setup described earlier.[50,51] Laser pulses with an energy of 3.7 nJ and a duration of 6 fs centered around 870 nm are generated from a commercial Ti:sapphire oscillator (Femtolasers Rainbow) operating at a repetition rate of 82 MHz. The pulse dispersion is controlled by a pair of chirped mirrors (Femtolasers GSM014, GDD = -45 fs^2/bounce) together with a pair of wedges (Femtolasers UA124, angle 2°48′, Suprasil 1) for fine adjustment. A dispersion-balanced Mach–Zehnder interferometer is used for generating a collinearly propagating pair of pulses with a variable time delay τ between them. This time delay is controlled with a precision of $\sim$50 as by means of a hardware-linearized single-axis piezo scanner (Physik Instrumente P-621.1CD PIHera). The pulse pair is expanded to a beam size of 15 mm in an all-reflective Kepler telescope and then focused onto the nanoslit grating on the gold taper to a spot size of 1–2 μm at close to normal incidence by using a dispersion-free,[32] all-reflective, aluminum-coated 36× Cassegrain microscope objective (Davin Optronics, 5004-000) with a numerical aperture (NA) of 0.5 and a working distance of 8.6 mm. In order to maximize the SPP coupling efficiency, the laser pulses are linearly polarized in the direction perpendicular to the nanoslit gratings. The scattered light from the tip is then collected by a second microscope objective (NA = 0.7) in reflection geometry, spectrally dispersed in a monochromator (SpectraPro-2500i, Acton), and detected with a deep-depletion liquid-nitrogen-cooled CCD detector (Spec-10 100-BR, Princeton Instruments) as a function of the time delay τ between both pulses. For adiabatically focused s-NSOM imaging[10] of metallic nanoparticles, the collected scattered light from the tip apex is imaged onto photodetector and a CDD camera while raster-scanning the tip across the sample surface.

Scattering-Type Near-Field Scanning Optical Microscopy (s-NSOM). s-NSOM imaging was performed in a home-built microscope described earlier.[10] Briefly, etched grating tapers are mounted onto a quartz tuning fork used as shear force sensor of the tip–sample distance. The grating is illuminated with sub-20 fs pulses centered around 800 nm from a home-built Ti:sapphire oscillator focused to a spot size of 3–4 μm using an microscope objective (Nikon SLWD 20×) with an NA of 0.35 and a working distance of 20 mm. Gold nanoparticles (BBInternational) are deposited at low concentration onto a quartz substrate by dip coating. The sample is mounted onto a 3D hardware-linearized piezo scanner (Physik Instrumente P-733) and is raster-scanned with respect to the tip at a constant tip–sample distance of 4 nm. The light scattered from the tip apex is collected using a second microscope (Nikon SLWD 50×, NA 0.5) mounted at an angle of 70° with respect to the tip axis using a photomultiplier tube or a liquid-nitrogen-cooled CCD detector.

Conflict of Interest: The authors declare no competing financial interest.

Acknowledgment. The authors gratefully acknowledge financial support by the Korea Foundation for International Cooperation of Science & Technology (Global Research Laboratory project, K20815000003). The work in Germany was supported by the DFG (SPP 1391 and DFG-NSF Materials) and by DARPA (QuBE project).

Supporting Information Available: The movie shows a three-dimensional finite difference time domain simulation of the local electric field intensity of a 6 fs pulse focused onto a nanoslit grating, the launched SPP wavepacket on a conical gold taper, the nanofocused spot at the taper apex, and the resulting scattering into the far-field. This material is available free of charge *via* the Internet at http://pubs.acs.org.

Note Added after ASAP Publication: This paper published ASAP on June 15, 2012. Figure 2 was replaced and several reference citations were changed. The revised version was reposted on June 20, 2012.

REFERENCES AND NOTES

1. Raether, H. *Surface Plasmons on Smooth and Rough Surfaces and on Gratings*; Springer-Verlag: New York, 1988; Vol. 111.
2. Kreibig, U.; Vollmer, M. *Optical Properties of Metal Clusters*; Springer-Verlag: Berlin, 1995; p 532.
3. Nerkararyan, K. V. Superfocusing of a Surface Polariton in a Wedge-like Structure. *Phys. Lett. A* **1997**, *237*, 103–105.
4. Babadjanyan, A. J.; Margaryan, N. L.; Nerkararyan, K. V. Superfocusing of Surface Polaritons in the Conical Structure. *J. Appl. Phys.* **2000**, *87*, 3785–3788.
5. Stockman, M. I. Nanofocusing of Optical Energy in Tapered Plasmonic Waveguides. *Phys. Rev. Lett.* **2004**, *93*, 137404.
6. Gramotnev, D. K. Adiabatic Nanofocusing of Plasmons by Sharp Metallic Grooves: Geometrical Optics Approach. *J. Appl. Phys.* **2005**, *98*, 104302.
7. Issa, N. A.; Guckenberger, R. Optical Nanofocusing on Tapered Metallic Waveguides. *Plasmonics* **2007**, *2*, 31–37.
8. Gramotnev, D. K.; Vogel, M. W.; Stockman, M. I. Optimized Nonadiabatic Nanofocusing of Plasmons by Tapered Metal Rods. *J. Appl. Phys.* **2008**, *104*, 034311.
9. Neacsu, C. C.; Berweger, S.; Olmon, R. L.; Saraf, L. V.; Ropers, C.; Raschke, M. B. Near-Field Localization in Plasmonic Superfocusing: A Nanoemitter on a Tip. *Nano Lett.* **2010**, *10*, 592–596.
10. Sadiq, D.; Shirdel, J.; Lee, J. S.; Selishcheva, E.; Park, N.; Lienau, C. Adiabatic Nanofocusing Scattering-Type Optical Nanoscopy of Individual Gold Nanoparticles. *Nano Lett.* **2011**, *11*, 1609–1613.
11. Berweger, S.; Atkin, J. M.; Olmon, R. L.; Raschke, M. B. Adiabatic Tip-Plasmon Focusing for Nano-Raman Spectroscopy. *J. Phys. Chem. Lett.* **2010**, *1*, 3427–3432.
12. Park, I. Y.; Kim, S.; Choi, J.; Lee, D. H.; Kim, Y. J.; Kling, M. F.; Stockman, M. I.; Kim, S. W. Plasmonic Generation of Ultrashort Extreme-Ultraviolet Light Pulses. *Nat. Photonics* **2011**, *5*, 678–682.
13. Gonzalez-Tudela, A.; Martin-Cano, D.; Moreno, E.; Martin-Moreno, L.; Tejedor, C.; Garcia-Vidal, F. J. Entanglement of Two Qubits Mediated by One-Dimensional Plasmonic Waveguides. *Phys. Rev. Lett.* **2011**, *106*, 020501.
14. Verhagen, E.; Kuipers, L.; Polman, A. Enhanced Nonlinear Optical Effects with a Tapered Plasmonic Waveguide. *Nano Lett.* **2007**, *7*, 334–337.
15. Verhagen, E.; Spasenovic, M.; Polman, A.; Kuipers, L. Nanowire Plasmon Excitation by Adiabatic Mode Transformation. *Phys. Rev. Lett.* **2009**, *102*, 203904.
16. Volkov, V. S.; Bozhevolnyi, S. I.; Rodrigo, S. G.; Martin-Moreno, L.; Garcia-Vidal, F. J.; Devaux, E.; Ebbesen, T. W. Nanofocusing with Channel Plasmon Polaritons. *Nano Lett.* **2009**, *9*, 1278–1282.
17. Ropers, C.; Neacsu, C. C.; Elsaesser, T.; Albrecht, M.; Raschke, M. B.; Lienau, C. Grating-Coupling of Surface Plasmons onto Metallic Tips: A Nanoconfined Light Source. *Nano Lett.* **2007**, *7*, 2784–2788.
18. Berweger, S.; Atkin, J. M.; Xu, X. J. G.; Olrnon, R. L.; Raschke, M. B. Femtosecond Nanofocusing with Full Optical Waveform Control. *Nano Lett.* **2011**, *11*, 4309–4313.
19. Durach, M.; Rusina, A.; Stockman, M. I. Toward Full Spatiotemporal Control on the Nanoscale. *Nano Lett.* **2007**, *7*, 3145–3149.
20. Li, X. T.; Stockman, M. I. Highly Efficient Spatiotemporal Coherent Control in Nanoplasmonics on a Nanometer-Femtosecond Scale by Time Reversal. *Phys. Rev. B* **2008**, *77*, 195109.
21. Lerosey, G.; de Rosny, J.; Tourin, A.; Derode, A.; Montaldo, G.; Fink, M. Time Reversal of Electromagnetic Waves. *Phys. Rev. Lett.* **2004**, *92*, 193904.
22. Durach, M.; Rusina, A.; Kling, M. F.; Stockman, M. I. Predicted Ultrafast Dynamic Metallization of Dielectric Nanofilms by Strong Single-Cycle Optical Fields. *Phys. Rev. Lett.* **2011**, *107*, 086602.
23. Roy, D.; Williams, C. M.; Mingard, K. Single-Crystal Gold Tip for Tip-Enhanced Raman Spectroscopy. *J. Vac. Sci. Technol., B* **2010**, *28*, 631–634.
24. Kuttge, M.; Vesseur, E. J. R.; Verhoeven, J.; Lezec, H. J.; Atwater, H. A.; Polman, A. Loss Mechanisms of Surface Plasmon Polaritons on Gold Probed by Cathodoluminescence Imaging Spectroscopy. *Appl. Phys. Lett.* **2008**, *93*, 113110.
25. Shchegrov, A. V.; Novikov, I. V.; Maradudin, A. A. Scattering of Surface Plasmon Polaritons by a Circularly Symmetric Surface Defect. *Phys. Rev. Lett.* **1997**, *78*, 4269–4272.
26. Maradudin, A. A.; Leskova, T. A.; Garcia-Guerrero, E. E.; Mendez, E. R. The Scattering of Surface Plasmon Polaritons by Nanoscale Surface Defects. *Low Temp. Phys.* **2010**, *36*, 815–820.
27. Sanchez-Gil, J. A.; Maradudin, A. A. Resonant Scattering of Surface-Plasmon Polariton Pulses by Nanoscale Metal Defects. *Opt. Lett.* **2003**, *28*, 2255–2257.
28. Nagpal, P.; Lindquist, N. C.; Oh, S. H.; Norris, D. J. Ultrasmooth Patterned Metals for Plasmonics and Metamaterials. *Science* **2009**, *325*, 594–597.
29. Huang, J. S.; Callegari, V.; Geisler, P.; Bruning, C.; Kern, J.; Prangsma, J. C.; Wu, X. F.; Feichtner, T.; Ziegler, J.; Weinmann, P.; *et al.* Atomically Flat Single-Crystalline Gold Nanostructures for Plasmonic Nanocircuitry. *Nat. Commun.* **2010**, *1*, 150.
30. Kim, D. S.; Hohng, S. C.; Malyarchuk, V.; Yoon, Y. C.; Ahn, Y. H.; Yee, K. J.; Park, J. W.; Kim, J.; Park, Q. H.; Lienau, C. Microscopic Origin of Surface-Plasmon Radiation in Plasmonic Band-Gap Nanostructures. *Phys. Rev. Lett.* **2003**, *91*, 143901.
31. Rewitz, C.; Keitzl, T.; Tuchscherer, P.; Huang, J. S.; Geisler, P.; Razinskas, G.; Hecht, B.; Brixner, T. Ultrafast Plasmon Propagation in Nanowires Characterized by Far-Field Spectral Interferometry. *Nano Lett.* **2012**, *12*, 45–49.
32. Piglosiewicz, B.; Sadiq, D.; Mascheck, M.; Schmidt, S.; Silies, M.; Vasa, P.; Lienau, C. Ultrasmall Bullets of Light: Focusing Few-Cycle Light Pulses to the Diffraction Limit. *Opt. Express* **2011**, *19*, 14451–14463.
33. Ropers, C.; Solli, D. R.; Schulz, C. P.; Lienau, C.; Elsaesser, T. Localized Multiphoton Emission of Femtosecond Electron Pulses from Metal Nanotips. *Phys. Rev. Lett.* **2007**, *98*, 043907.
34. Beversluis, M. R.; Bouhelier, A.; Novotny, L. Continuum Generation from Single Gold Nanostructures through Near-Field Mediated Intraband Transitions. *Phys. Rev. B* **2003**, *68*, 115433.
35. Bouhelier, A.; Beversluis, M.; Hartschuh, A.; Novotny, L. Near-Field Second-Harmonic Generation Induced by Local Field Enhancement. *Phys. Rev. Lett.* **2003**, *90*, 013903.
36. Shen, Y. R. Optical 2nd Harmonic-Generation at Interfaces. *Annu. Rev. Phys. Chem.* **1989**, *40*, 327–350.
37. Heinz, T. F. Second-Order Nonlinear Optical Effects at Surfaces and Interfaces. In *Nonlinear Surface Electromagnetic Phenomena*; Ponath, H.-E., Stegeman, G. I., Eds.; North-Holland: Amsterdam, 1991; p 353.
38. Neacsu, C. C.; Reider, G. A.; Raschke, M. B. Second-Harmonic Generation from Nanoscopic Metal Tips: Symmetry Selection Rules for Single Asymmetric Nanostructures. *Phys. Rev. B* **2005**, *71*, 201402.
39. Garcia-Etxarri, A.; Romero, I.; de Abajo, F. J. G.; Hillenbrand, R.; Aizpurua, J. Influence of the Tip in Near-Field Imaging of Nanoparticle Plasmonic Modes: Weak and Strong Coupling Regimes. *Phys. Rev. B* **2009**, *79*, 125439.
40. Giannini, V.; Fernandez-Dominguez, A. I.; Heck, S. C.; Maier, S. A. Plasmonic Nanoantennas: Fundamentals and Their Use in Controlling the Radiative Properties of Nanoemitters. *Chem. Rev.* **2011**, *111*, 3888–3912.
41. Deeb, C.; Bachelot, R.; Plain, J.; Baudrion, A. L.; Jradi, S.; Bouhelier, A.; Soppera, O.; Jain, P. K.; Huang, L. B.; Ecoffet, C.; *et al.* Quantitative Analysis of Localized Surface Plasmons Based on Molecular Probing. *ACS Nano* **2010**, *4*, 4579–4586.

42. Lee, K. G.; Kihm, H. W.; Kihm, J. E.; Choi, W. J.; Kim, H.; Ropers, C.; Park, D. J.; Yoon, Y. C.; Choi, S. B.; Woo, H.; *et al.* Vector Field Microscopic Imaging of Light. *Nat. Photonics* **2007**, *1*, 53–56.
43. Dereux, A.; Girard, C.; Weeber, J. C. Theoretical Principles of Near-Field Optical Microscopies and Spectroscopies. *J. Chem. Phys.* **2000**, *112*, 7775–7789.
44. Chicanne, C.; David, T.; Quidant, R.; Weeber, J. C.; Lacroute, Y.; Bourillot, E.; Dereux, A.; des Francs, G. C.; Girard, C. Imaging the Local Density of States of Optical Corrals. *Phys. Rev. Lett.* **2002**, 88.
45. Amat-Roldan, I.; Cormack, I. G.; Loza-Alvarez, P.; Gualda, E. J.; Artigas, D. Ultrashort Pulse Characterisation with SHG Collinear-Frog. *Opt. Express* **2004**, *12*, 1169–1178.
46. Stibenz, G.; Steinmeyer, G. Interferometric Frequency-Resolved Optical Gating. *Opt. Express* **2005**, *13*, 2617–2626.
47. Stibenz, G.; Ropers, C.; Lienau, C.; Warmuth, C.; Wyatt, A. S.; Walmsley, I. A.; Steinmeyer, G. Advanced Methods for the Characterization of Few-Cycle Light Pulses: A Comparison. *Appl. Phys. B* **2006**, *83*, 511–519.
48. Tritschler, T.; Mucke, O. D.; Wegener, M.; Morgner, U.; Kartner, F. X. Evidence for Third-Harmonic Generation in Disguise of Second-Harmonic Generation in Extreme Nonlinear Optics. *Phys. Rev. Lett.* **2003**, 90.
49. Anderson, A.; Deryckx, K. S.; Xu, X. J. G.; Steinmeyer, G.; Raschke, M. B. Few-Femtosecond Plasmon Dephasing of a Single Metallic Nanostructure from Optical Response Function Reconstruction by Interferometric Frequency Resolved Optical Gating. *Nano Lett.* **2010**, *10*, 2519–2524.
50. Schmidt, S.; Mascheck, M.; Silies, M.; Yatsui, T.; Kitamura, K.; Ohtsu, M.; Lienau, C. Distinguishing between Ultrafast Optical Harmonic Generation and Multi-Photon-Induced Luminescence from ZnO Thin Films by Frequency-Resolved Interferometric Autocorrelation Microscopy. *Opt. Express* **2010**, *18*, 25016–25028.
51. Mascheck, M.; Schmidt, S.; Silies, M.; Yatsui, T.; Kitamura, K.; Ohtsu, M.; Leipold, D.; Runge, E.; Lienau, C. Observing the Localization of Light in Space and Time by Ultrafast Second-Harmonic Microscopy. *Nat. Photonics* **2012**, *6*, 293–298.
52. Samson, Z. L.; Horak, P.; MacDonald, K. F.; Zheludev, N. I. Femtosecond Surface Plasmon Pulse Propagation. *Opt. Lett.* **2011**, *36*, 250–252.
53. Qian, H. *Tip-Enhanced Near-Field Optical Spectroscopy on Single-Walled Carbon Nanotubes*; Ludwig-Maximilians-Universität: München, Germany, 2008.